Faecalibaculum rodentium-derived ACT domain protein suppresses CRC development via reducing SLC25A22-mediated glutamate metabolism

Yu Cheng[1#], Ruihan Jiang[1#], Hanyong Zhu[1], Yuhang Xue[1], Can Zhou[1], Luohang Huang[3], Guojiao Zhu[3], Hui Guo[1], Binbin Ji[1], Miaomiao Sun[1], Yuchen Pan[1,3*], Jing Han[2*], Jing Yang[1,3*]

[1]Jiangsu Key Laboratory of Immunity and Metabolism, The Department of Pathogenic Biology and Immunology, School of Basic Medical and Life Sciences, Xuzhou Medical University, Xuzhou, Jiangsu, China; [2]Department of Clinical laboratory Medicine, Jiangnan University Medical Center, Wuxi, Jiangsu, China; [3]National Demonstration Center for Experimental Basic Medical Science Education, Xuzhou Medical University, Xuzhou, Jiangsu, China.

# These authors contributed equally to the work.
Running title: *F. rodentium*-derived ACT protein inhibits CRC

Address for correspondence:
Jiangsu Province Key Laboratory of Immunity and Metabolism, The Department of Pathogenic Biology and Immunology, Xuzhou Medical University, 209 Tongshan Road, Xuzhou, 221004, Jiangsu, China
Jing Yang, e-mail: jingyang@xzhmu.edu.cn
Yuchen Pan, e-mail: panyuchen@xzhmu.edu.cn

Department of Clinical laboratory Medicine, Jiangnan University Medical Center (Wuxi No.2 People's Hospital), Wuxi, Jiangsu, China
Jing Han, e-mail: Hjing1994@163.com

Abstract

Probiotics exert anti-tumor effects against colorectal cancer (CRC) through multiple pathways, yet their translation into clinical practice remains challenging. Identifying the specific tumor-suppressive molecules derived from these probiotics and their host targets is a promising strategy to address this challenge. We identified the aspartate kinase, chorismate mutase, and prephenate dehydrogenase (TyrA) domain protein (hereafter termed ACT protein) derived from *Faecalibaculum rodentium* and demonstrated that ACT protein impeded the formation of patient-derived CRC organoids and suppressed CRC growth and metastasis *in vivo* without overt side effects. Mechanistically, the ACT protein transported into cells via macropinocytosis and directly bound to the mitochondrial glutamate transporter SLC25A22 in CRC cells, leading to decreased SLC25A22-mediated glutamate transport and metabolism, along with reduced level of α-ketoglutarate (α-KG), a metabolic intermediate of glutamate. Conversely, ectopic expression of SLC25A22 or exogenous α-KG supplementation attenuated the growth-inhibitory effect of the ACT protein. Collectively, these observations indicate that ACT protein suppresses CRC growth by directly targeting SLC25A22 and reducing its glutamate transport activity; positioning ACT protein as a candidate inhibitor of SLC25A22 with potential for further translational development.

Keywords: *F. rodentium*, ACT domain protein, CRC, SLC25A22

Introduction

Colorectal cancer (CRC) persists as a major global health challenge, ranking among the most frequently diagnosed malignancies and a leading cause of cancer-related mortality [1]. While prognostic and therapeutic improvements have been achieved, long-term survival rates remain unsatisfactory, underscoring the urgent need for innovative treatment strategies [2]. Emerging evidence now highlight the gut microbiota as an important factor influencing CRC pathogenesis, disease progression, and therapeutic efficacy, positioning it as a promising frontier for novel interventions [3-5].

The gut microbiota acts as a double-edged sword in CRC development. On one hand, gut microbiome such as *Fusobacterium nucleatum* [6-8] and certain strains of *Escherichia coli* (e.g., pks+ *E. coli*) [9], directly promote carcinogenesis by regulating several pathways. On the other hand, commensal bacteria such as *Faecalibaculum rodentium* (*F. rodentium*) and *Faecalibacterium prausnitzii*, through the production of short-chain fatty acids like butyrate, maintain intestinal epithelial integrity, suppress inflammation, and induce anti-tumorigenic effects [10-12]. Beyond SCFAs, several studies have revealed a plethora of other metabolites or secreted molecules with anti-tumor effects [3]. *Lactobacillus gallinarum* reduces both the number and size of colorectal tumors via its protective metabolites indole-3-lactic acid (ILA) in $Apc^{Min/+}$ and chemically induced CRC mouse models [13]. *Lactobacillus reuteri*-derived reuterin blocks CRC growth *in vitro* and *in vivo* via suppression

of protein translation [14]. Both *Akkermansia muciniphila* and the specific protein in *Akkermansia muciniphila,* Amuc_1100 blunts tumourigenesis [15]. Likewise, *Streptococcus thermophilus*-derived β-galactosidase suppresses CRC development via reprogramming cancer cell metabolism [16].

Besides directly inducing CRC suppression, gut microbiota potentiates the anti-tumor ability of chemotherapy and immune checkpoint inhibitors (ICI) response via enhancing immune surveillance. The gut microbiota enhances the anti-tumor ability of cyclophosphamide through stimulating the generation of "pathogenic" Th17 cells and memory Th1 immune responses [17]. The mixture of 11 bacterial strains enhances the therapeutic efficacy of ICIs such as anti-PD1 antibody in syngeneic tumour models [18]. Collectively, these observations indicate that the gut flora provides a rich and highly diverse repertoire of tumour-suppressive molecules. Given the challenge of achieving stable engraftment of live bacterial therapeutics in the gut, identifying and investigating the potential secreted molecules of the microbiota offers a crucial alternative path toward the therapeutic treatment of CRC.

Beyond its role in alleviating ionizing radiation-induced damage [19], *F. rodentium* has been shown to inhibit CRC growth, an effect largely attributed to its production of short-chain fatty acids [20]. Nevertheless, it remains unclear whether the bacterial culture medium contains additional, undiscovered tumor-suppressive molecules. Therefore, in this study, we investigate the anti-tumor effects of the *F. rodentium* and its culture medium to identify any

potential secreted effector molecules, and to elucidate the underlying mechanisms responsible for its anti-tumor activity. We identified aspartate kinase, chorismate mutase, and prephenate dehydrogenase (TyrA) domain protein (hereafter termed ACT protein) harboring anti-tumor ability from *F. rodentium* culture medium (FCM), and found that ACT protein inhibited CRC development via directly binding to the mitochondrial glutamate transporter solute carrier family 25 member 22 (SLC25A22), and attenuating SLC25A22-mediated glutamate transport and metabolism.

Results

F. rodentium/FCM suppresses CRC development by reducing glutamate metabolism.

Previous study showed that *F. rodentium* inhibited CRC progression via its metabolite butyrate. Consistent with this tumor-suppressive role, in this study we found that the tumor number and tumor size were increased in AOM/DSS-treated *Rosa26*$^{mSTAT3/mSTAT3}$;*Villin*$^{Cre/+}$ mice (**Fig.1A-D**) which exhibited reduced *F. rodentium* abundance [19]. Conversely, both *F. rodentium* and FCM reduced tumor size and tumor weight (**Fig.1E-H**). Unexpectedly, heat-inactivated *F. rodentium* & FCM (HFr) attenuated the anti-tumor effects of *F. rodentium* or FCM (**Fig.1E-H**), indicating that other key anti-tumor factors besides butyrate exist in FCM.

Given the gut microbiota modulates host metabolic reprogramming through microbial metabolites and/or derived molecules, directly or indirectly influencing energy supply, cellular metabolic states and immune responses. Therefore, we performed untargeted metabolomics analysis and found that the three experimental groups (ctrl, *F. rodentium*/FCM, and HFr) were clear separated, although the metabolite profiles overlapped between *F. rodentium*- and FCM-treated mice (**Fig. 1I**), suggesting that microbial metabolites in the *F. rodentium* or FCM treatment differ substantially from those in the control culture medium or HFr groups. We analyzed differential metabolites between every pair of treatment groups and identified 680 differentially abundant

metabolites common to *F. rodentium* and FCM treatments (**Fig. 1J**). KEGG pathway classification highlighted the amino acid metabolism among these metabolites, with specific enrichment in glutamate/alanine/aspartate metabolism (**Fig. 1K-L**).

Glutamate functions as a central metabolic node, providing both energy and biosynthetic precursors to fuel tumor growth and survival [21, 22]. Given that glutamate is rapidly metabolized and exhibits excitotoxicity, its precursor glutamine is used in rescue experiments to functionally validate the role of glutamate in FCM-mediated tumor suppression, we supplemented tumor-bearing mice with dietary or water-soluble glutamine, and found that glutamine supplementation significantly diminished the anti-tumor effect of *F. rodentium* and FCM (**Fig. 1M-O**). These observations demonstrated that *F. rodentium* could suppress CRC growth, at least in part, by reducing glutamate metabolism, an effect which is mediated by bioactive molecules present in FCM.

***F. rodentium*-derived ACT protein inhibits CRC growth *in vitro* and *in vivo*.**

To confirm if bioactive molecules are present in FCM, we performed colony assay and found that FCM, but not the heated FCM (hFCM) inhibited colony formation in CRC cell lines, and concurrently lowered the levels of α-KG and succinic acid, the downstream metabolites of glutamate within these cells (**Fig. 2A-B**).

To identify the specific molecule in FCM responsible for lowering glutamate metabolism, we performed LC/MS analysis and identified a secreted product with the smallest molecular weight (approximately 15 kDa), which was an ACT domain-containing protein (**Fig. 2C**). To evaluate the function of this ACT protein, we established doxycycline-inducible ACT expression in HCT-8, SW480 and HCT-8R cell lines using a Tet-on system. Ectopic expression of the ACT protein from *F. rodentium* significantly suppressed colony formation, whereas expression of the homologous ACT protein from *Holdemanella biformis* (a human gut commensal, HACT) or ACT protein from *Dubosiella muris* (DACT) barely affected the colony formation (**Fig. 2D-G**). Furthermore, induced ACT expression markedly inhibited HCT-8 metastasis *in vivo* (**Fig. 2H-I**).

We also produced and purified recombinant His-tagged ACT protein (rACT) from *E. coli*. The colony formation assay is the gold standard for assessing long-term proliferative capacity and reproductive integrity [23], and RTCA allows real-time monitoring of the cell index. We therefore performed colony formation assay in FHC cells to assess the potential side effects of rACT and in SW480 cells harboring KRAS mutations to examine its anti-tumor activity. We found that rACT did not affect FHC cell proliferation (**Fig. 3A**). whereas it markedly inhibited the proliferation of SW480 cells (**Fig. 3B**). *In vivo,* rACT significantly reduced the tumor size without impairing cognitive function in mice (**Fig. 3C-J**). In addition, in mice injected with rACT via the tail vein, His-tag

levels were detected in tumor tissues but not major organs such as liver and spleen, indicating favorable tumor tissue permeability of rACT (**Fig. 3K-M**). Importantly, patient-derived organoid (PDO) were sensitive to rACT (**Fig. 3N**). Collectively, these results demonstrated that the ACT protein secreted by *F. rodentium* is a key functional mediator that inhibits CRC growth.

ACT protein could enter tumor cells via macropinocytosis.

Protein entry into tumor cells can occur through classical endocytic pathways including macropinocytosis and clathrin-mediated endocytosis [24, 25], or through non-classical mechanisms such as direct membrane translocation and energy-independent passive internalization [26, 27]. To determine which pathway mediated rACT uptake, we treated HCT-8 and SW480 cells with rACT in the presence or absence of Amiloride hydrochloride or Cytochalasin D to inhibit macropinocytosis. Both inhibitors blocked ACT protein entryinto tumor cells (**Fig. 4A-B**). In contrast, Dynasore, which blocks clathrin-mediated endocytosis, did not affect ACT protein entry. Furthermore, incubation cells at 4 ° C reduced ACT protein internalization (**Fig. 4A-B**). These observations suggested that ACT protein could enter CRC cells via an energy-dependent, and clathrin-independent mechanism, most likely macropinocytosis, which should be investigated in future study.

ACT protein directly interacts with SLC25A22.

Since at the cellular level, glutamate metabolism occurs primarily in the mitochondria, where glutamate is converted to α-KG, linking amino acid

metabolism to the TCA cycle and urea cycle. We utilized Co-IP together with LC/MS to identify the corresponding receptor responsible for ACT protein. 76 mitochondrial proteins have been found (**Fig. 5A**). Among these proteins, mitochondrial inner membrane especially the mitochondrial glutamate transporter such as SLC25A22 were enriched in gene ontology (GO) enrichment (**Fig. 5B-C**). Since SLC25A11 mediates the exchange of ketoglutarate with other dicarboxylates [28]. SLC25A10 drives the polarization of tumor-associated macrophages toward a pro-tumor phenotype by promoting succinate transport, thereby driving CRC progression [29]. SLC25A6 is responsible for the exchange of ADP and ATP, as well as the opening of the mitochondrial permeability transition pore [30]. Unlike these members, SLC25A22 is a key glutamate transporter whose expression levels are elevated in CRC, especially in tumors harboring KRAS mutations [31-33] rather than in tumor-infiltrating immune cells (**Fig. 5D**), and it is closely associated with tumor progression [31-33]. We hypothesized that the ACT protein could interact with SLC25A22 to regulate glutamate metabolism.

The protein interaction prediction showed that ACT protein could bind to both the glutamine importer SLC1A5 and the glutamate transporter SLC25A22 (**Fig. 5E**). However, co-IP results showed that ACT protein from *F. rodentium* but not from *Holdemanella biformis* or *Dubosiella muris,* bound to SLC25A22, rather than to SLC1A5 (**Fig. 5F-G**). Interestingly, the $SLC25A22^{T74A}$ and $SLC25A22^{I183A/S187A}$ double mutant showed impaired binding to Flag-ACT (**Fig.**

5H). Immunofluorescence (IF) showed that ACT protein co-localized with SLC25A22 (**Fig. 5I**). Of note, BLI experiment also revealed that His-tagged rACT bound to SLC25A22 (**Fig. 5J**). To confirm the role of SLC25A22 in rACT-mediated tumor suppression, we ectopic expressed SLC25A22 in HCT-8 cells harboring wild-type KRAS and found that the growth inhibition induced by ACT protein was attenuated (**Fig. 5K**), indicating that ACT protein can directly interact with SLC25A22 to inhibit CRC growth.

ACT protein reduces SLC25A22-mediated glutamate transport and metabolism.

To validate the dependence of rACT-mediated tumor suppression on SLC25A22-mediated glutamate transport and metabolism, we examined glutamate transport and found that rACT reduced FITC-glutamate uptake in CRC cell lines (**Fig. 6A-B**). In addition, ^{13}C-glutamate metabolic flux analysis revealed that upon rACT treatment, the levels of ^{13}C-glutamate, ^{13}C-glutamine, and TCA cycle intermediates such as fumaric acid and isocitric acid were reduced without affecting glycolysis (**Fig. 6C-D**). Since ^{13}C-labeling primarily reflects carbon flux rather than total metabolite pool size. Additionally, α-KG and succinic acid are not only TCA cycle intermediates but also key regulators of epigenetic states and tumor progression [34, 35]. We next directly measured the total intracellular levels of α-KG and succinic acid and found that the levels of both α-KG and succinic acid were decreased following rACT treatment (**Fig. 6E**). Additionally, upon ACT treatment, the basal and maximal OCRs were

reduced in both HCT-8 and SW480 cells (**Fig. 6F-G**). These observations demonstrated that ACT protein binds to SLC25A22 and reduces SLC25A22-mediated glutamate transport and metabolism.

We next sought to determine which metabolite is critical for rACT-induced CRC suppression. To this end, we treated SW480 cells with α-KG or succinic acid in the presence or absence of rACT. We found that α-KG but not succinic acid abrogated the anti-tumor ability of rACT (**Fig. 6H**). Similarly, this rescue effect was further validated in PDOs with mutant KRAS, in which α-KG also attenuated rACT-mediated tumor suppression (**Fig. 6I**). Collectively, these results clarified the direct interplay between ACT protein and SLC25A22, ACT protein directly binds to SLC25A22, inhibits SLC25A22-mediated glutamate transport and metabolism, and thereby suppresses CRC development (**Fig. 7**).

Discussion

The gut microbiota and its metabolic products have been increasingly recognized as causal and mechanistic contributors to CRC initiation, progression, and therapeutic responsiveness [3-5], underscoring the imperative to integrate gut microbial metabolism into targeted interventions for CRC patients. A range of microbiota-centered strategies, including dietary modulation, prebiotics, probiotics, postbiotics, engineered live biotherapeutics, and fecal microbiota transplantation, are currently being developed for precision prevention and therapy [36-40]. Collectively, these advances highlight the therapeutic promise of microbiota-derived metabolites, positioning the gut microbiome as a compelling axis for combination regimens that synergize microbial modulation with conventional and immunotherapeutic approaches. Nevertheless, the clinical translation of probiotics remains hindered by substantial obstacles, notably the inefficiency of microbial colonization [41-43]. Identifying the key anti-tumor bioactive components derived from probiotics represents a key and actionable breakthrough.

We previously found that *F. rodentium* protected mice from irradiation-induced damage [19]. Previous studies also found that *F. rodentium* inhibited CRC development by its metabolite short chain fatty acids (SCFAs) [20, 44]. However, whether *F. rodentium* produces additional anti-tumor components or metabolites beyond SCFAs remains largely unexplored. As the gut flora becomes increasingly entrenched as a pivotal modulator of tumor biology,

microbial-derived functional proteins have risen to the forefront of cancer research. Herein, in the present study, we aimed to explore the potential anti-tumor molecules derived from *F. rodentium* and found that ACT protein obviously suppressed CRC development (**Fig. 2-6**).

The ACT domain is a conserved regulatory module and commonly found in a wide range of bacterial proteins involved in amino acid metabolism and signal transduction [45, 46]. It functionally serves as a small-molecule binding module, typically sensing amino acids or other ligands to allosterically regulate the activity of its host enzyme [45, 47]. While the functions of bacterial ACT protein are unclear in tumor biology.

In the study, our data showed that intravenously injected rACT efficiently suppressed tumor growth along with ACT protein accumulated in tumor tissues without producing detectable impairment of cognitive function in mice (**Fig. 3**), suggesting ACT protein harbors the anti-tumor effects with favorable tissue permeability and a reassuring safety profile. Mechanistically, we found that ACT protein entered cells via non-classical mechanisms, directly engaged SLC25A22 and reduced SLC2A22-mediated glutamate transport and metabolism (**Fig. 4-6**), culminating in potent inhibition of CRC development (**Fig. 7**).

SLC25A22, a mitochondrial inner membrane glutamate transporter, has emerged as a critical metabolic dependency in CRC, particularly in the context of KRAS mutations [32, 33]. SLC25A22 mediates the mitochondrial import of

glutamate, which is essential for glutaminolysis and the maintenance of mitochondrial metabolism. In CRC cells with mutant KRAS, SLC25A22-mediated glutaminolysis promotes the accumulation of succinate, resulting in increased DNA methylation, activation of WNT signaling to β-catenin, and enhanced stemness and drug resistance [32, 33]. SLC25A22 also promotes proliferation and survival of CRC cells with KRAS mutations and xenograft tumor progression in mice via intracellular synthesis of aspartate [33]. Moreover, SLC25A22 has been identified as a metabolic suppressor of ferroptosis by maintaining glutathione production [48], further expanding its role in cancer cell survival. Importantly, CRC patients with elevated levels of SLC25A22 have significantly shorter survival times [33]. A combinatorial approach utilizing SLC25A22 shRNA plus 5-fluorouracil synergistically suppresses KRAS-mutant CRC growth [32]. Additionally, targeting SLC25A22 has been shown to revert KRAS-mediated immunosuppression in pre-clinical CRC models by suppressing CXCL1 production and impairing myeloid-derived suppressor cell (MDSC) recruitment, and the combination of SLC25A22 targeting with anti-PD-1 therapy synergistically suppresses KRAS-mutant CRC growth [31].

Despite the growing recognition of SLC25A22 as a encouraging therapeutic target, the development of small-molecule inhibitors specifically targeting SLC25A22 remains in its early stages. The structural challenges associated with targeting mitochondrial inner membrane transporters, including their

hydrophobic nature, and limited accessibility, have hindered the development of selective small-molecule inhibitors. Currently, no clinically approved small-molecule inhibitor of SLC25A22 is available. Most studies have relied on genetic approaches such as shRNA or CRISPR-mediated knockout to validate the functional consequences of SLC25A22 inhibition [32, 49]. Unexpectedly, our results indicated that ACT protein derived from *F. rodentium* but not other bacteria can be a potential promising inhibitor of SLC25A22 (**Fig. 2-6**), and the anti-tumor effects of ACT protein should be investigated in a larger number of PDO with KRAS mutation or KRAS-mutant CRC patients. Moreover, the amino acid residues of ACT protein required for its anti-tumor effects warrant further investigation in future study.

Limitations

Compared with conventional chemical drugs or gene-based therapies, ACT protein offers several notable advantages, including lower systemic toxicity. Nevertheless, its clinical translation faces considerable challenges. First, at the molecular level, since our mutagenesis data have not identified the important residues in SLC25A22, elucidating the precise structural basis underlying the ACT-SLC25A22 interaction will be essential for guiding rational drug design. In addition, unlike its homologs from other gut commensals such as *Holdemanella biformis* or *Dubosiella muris*, the specific amino acid determinants responsible for the anti-tumor activity of *F. rodentium*-derived ACT remain to be characterized. Second, at the cellular level, the mechanism

underlying the entry of ACT protein into tumor cells remains uncharacterized. Moreover, the mechanisms underlying the preferential localization of His-tagged ACT protein in tumor tissues rather than in normal organs remain unclear. Third, at the systemic level, the foremost challenge is the need for a systematic evaluation of its immunogenicity, given the bacterial origin of the protein. The pharmacokinetic properties and long-term safety of ACT protein following parenteral administration have yet to be fully defined. Furthermore, it remains uncertain whether the anti-tumor efficacy observed in preclinical models can be recapitulated in human patients. Whether this ACT protein exerts similar effects in other cancer types or under distinct genetic contexts also warrants further exploration. Finally, the potential role of the gut microbiota in modulating the therapeutic efficacy of ACT-mediated therapy was not directly examined in this study. Addressing these limitations will be critical for translating the mechanistic insights into clinically viable therapeutic strategies.

Conclusions

In conclusion, by binding to SLC25A22 and suppressing its glutamate transport and metabolism, ACT protein reduces intracellular α-KG levels and inhibits tumor growth. These findings could support ACT protein as both a promising SLC25A22 inhibitor and a potential precision therapeutic for KRAS-mutant CRC. Future studies should focus on elucidating this entry mechanism to guide rational drug design and delivery.

Materials and Methods

PDOs culture

Human CRC organoids were purchased from Fcmacs Biotech Co., Ltd (Nanjing，China), and photographed at the proper times. For passage of tumor organoids, the Matrigel containing organoids were pipetted into 15 mL centrifuge tube using ice-cold PBS and washed with centrifugation at 500 g. The suspension was removed and the pellets were resuspended in ice-cold PBS with pipetting 30–60 times using a 1 mL pipette. The cell mixture was washed and embedded in Matrigel at a 1:2 ratio. The culture medium was changed every 3 d.

Mice

Rosa26$^{mSTAT3/mSTAT3}$ knock-in mice were lab stock, and crossed with *Villin*$^{Cre/+}$ mice (Shanghai Model Organisms Center, Inc., Shanghai, China) to obtain *Rosa26*$^{mSTAT3/mSTAT3}$*;Villin*$^{Cre/+}$ mice. C57BL/6 (B6) (CD45.2) mice were obtained from Cavens Laboratory Animal Co., Ltd. (Changzhou, China). NSG mice were kind gift from professor Renjin Chen (Xuzhou Medical university). Mice were strictly bred and maintained under protocols approved by the Institutional Animal Care and Use Committee at Xuzhou Medical University (Approval No. 202104A077, 202303T015). Mice were daily monitored for general activity, and respiratory status throughout the study. Humane endpoints were applied in accordance with institutional guidelines, and mice were humanely euthanized at the end of the experiment or when predefined ethical criteria

including tumor volume reached 1,000 mm^3 were met. The investigator was not blinded to the group allocation of the animals during the experiment. No statistical method was used to predetermine the sample size for the mice experiment, which was based on preliminary experimental results. The sample size of each experiment is shown in the legend.

AOM/DSS-induced colitis-associated colorectal cancer

Briefly, 8-12 week-old mice of body weight > 20 g were i.p. injected of azoxymethane (AOM, 10 mg/kg body weight). After 7 days, mice were treated with 2% dextran sodium sulfate (DSS) in drinking water for 7 days, and followed by normal drinking water for another 14 days. Three cycles of DSS treatment were needed before tumor evaluation. On day 63 of the regime, the intestinal and colon sections were removed, washed with PBS and opened longitudinally for analysis.

Ectopic tumor implantation and weight measurements

Tumor implantation and weight measurements were performed as previously described [50].

Glutamine supplementation was administered via diet or drinking water as described [51]. The supplemented diet was prepared by adding 200 g of glutamine to the standard chow, with a daily provision of 0.5 g per cage. For supplementation in water, an equivalent amount of glutamine was dissolved in the drinking water and changed daily.

For ACT domain protein treatment experiment, 1×10^6 MC-38 cells were s.c.

implantated as described [50]. When a palpable tumor formed, the mice were treated with either the same volume of control diluent, 100 μg/tumor (every other day) or 5 mg/kg ACT (every other day, i.v. injection), respectively.

Lung metastasis model

HCT-8-ACT cells were injected into NSG mice (kindly gift from professor Renjin Chen, Xuzhou Medical Univeristy) via tail vein. 7 days later, mice were administrated with either normal water or containing 2 mg/mL DOX water. After 21 days, the mice were euthanized, and lungs were removed, and embedded in paraffin for H&E staining.

Cell culture

Human colorectal cancer SW480 and HCT-8 cell line were commercially obtained from the Chinese Academy of Sciences Committee on Type Culture Collection Cell Bank (SCST, Shanghai, China). HCT-8R (alisertib resistance) cell line was established as decribed previously [52]. CRC cell lines were maintained in Dulbecco's modified Eagle's medium (DMEM) containing 10% heat-inactivated FBS, 100 mg/L streptomycin and 100 U/mL penicillin at 37 °C in a 5% CO_2 environment. Murine MC-38 cells and human HET-293T cells were purchased from FuHeng (FuHeng Cell Center, Shanghai, China) and maintained in DMEM supplemented with 10% FBS.

Reagents

Doxycycline (DOX, HY-N0565), α-KG (HY-W013636), succinic acid (HY-N0420), FCCP (HY-100410) and puromycin were obtained from MCE

(Shanghai, China). Ligomycin (103592-100) and Rotenone/Antimycin A (103592-100) were obtained from Agilent Technology. Dynasore (T1848), Amiloride hydrochloride (T0175) and Cytochalasin D (T3229) were purchased from TargetMol (Shanghai, China).

Plasmid DNA, lentivirus, and infection

pcDNA3.1-flag-SLC25A22 plasmid DNA was purchased from HonorGene. The SLC25A22^{T74A}, and SLC25A22$^{I813A/S187A}$ double mutants were constructed as described previously [53]. Primer sequences were provided in Supplementary Table S1.

The baterial ACT domain protein cDNAs were amplified and cloned into either pcDNA3.1 vector or the pLVX-TetOne-Puro vector. Lentiviruses were generated and stable cell lines were established as described previously [54].

Generation of ACT and SLC25A22 protein

Briefly, ACT domain protein cDNA expression vector was constructed by inserting the fragment carrying the *F. rodentium* ACT cDNA between the NcoI and XhoI sites of the pET28a expression vector (Xuzhou, China). SLC25A22 cDNA expression vector was constructed by inserting the fragment between the BamHI and XhoI sites of the pET32T expression vector, and mutant SLC25A22 expression vectors were generated as described previously [53]. The indicated expression vector were transformed into ArcticExpress competent cells and incubated with isopropyl-1-thio-β-D-galactopyranoside (IPTG) (final concentration was 0.5 mM) at 37 °C for 4 h with shaking. Then,

the fusion protein was purified by Ni-iminodiacetic acid (IDA) affinity chromatography. The purified protein was confirmed by CBB staining and Immunoblotting analysis [55]. The endotoxin content of the purified protein is less than 0.1EU/mL.

Bio-Layer Interferometry (BLI) assay

Binding interactions between ACT protein and SLC25A22 were measured by bio-layer interferometry (BLI) using an Octet system (Sartorius) equipped with HIS1K biosensors. Both protein immobilization and binding assays were conducted in 1.0×PBS (pH 7.4). Prior to use, biosensors were pre-hydrated in 1.0×PBS for at least 10 min. ACT protein was diluted to 100 μg/mL in 1.0×PBS and immobilized onto the sensors via amine coupling for 100 s, yielding an immobilization level of approximately 1 nm. Reference sensors were prepared in parallel using protein-free buffer under identical conditions.

For affinity measurements, SLC25A22 protein were serially diluted in 1.0×PBS in a 96-well plate. The protein-coupled sensors were sequentially exposed to SLC25A22 protein at ascending concentrations. Association and dissociation phases were monitored for 120 s and 180 s, respectively, with buffer washes between each concentration step. The binding sensorgrams were analyzed using Octet® BLI Analysis software (Sartorius) and globally fitted to a 1:1 steady-state affinity binding model to determine the equilibrium dissociation constants.

Cell proliferation assay

Cell proliferation was monitored in real time by using an xCELLgence RTCA DPlus system (Agilent Technology). CRC cells were seeded in an E-plate 16 at a density of 5000 cells per well and locked in an RTCA device at 37°C with 5% CO_2. The cell index was monitored and recorded in real time every 30 min for 24 h.

Colony formation assay

The colony formation assay was performed as previously described [55].

Metabolic Flux Analysis

Cells were treated with or without rACT (1 μg/mL) for 24 h, and followed by incubation in DMEM in the presence of 2 mM ^{13}C5-glutamate for another 2 h. The cells were harvested and washed with ice-cold saline before being snap-frozen on dry ice, and fast quenched with −80 °C pre-cooled extraction solution [methanol/acetonitrile/water (2:2:1, v/v)]. After being incubated at −40 °C, the samples were vortexed followed by centrifugation at 4 °C. The supernatants were collected and evaporated. The dried extracts were reconstituted in acetonitrile/water (1:1, v/v) solution, followed by sonication and centrifugation to remove insoluble materials. Metabolites were analyzed on a Thermo Vanquish UHPLC system by Shanghai Biotree biomedical technology (Shanghai, China).

Metabolomics analysis

For untargeted metabolomics analysis, the contents of the cecum of mice were harvested and subjected to untargeted metabolomics sequencing by Majorbio

(Shanghai, China). The data were analyzed using the Majorbio Cloud Platform (www.majorbio.com).

α-KG levels in the cells or serum were examined using α-Ketoglutarate (α-KG) Content Assay Kit (ADS-W-S012, AIDISHENG, Yancheng, Jiangsu, China) according to the manufacturer's instructions.

Succinic acid levels in the cells were examined using Amplex Red Succinate Assay Kit (S0529S, Beyotime, Shanghai, China) according to the manufacturer's instructions.

Metabolic Assays

The OCR were measured with an XF 24 extracellular flux analyzer (Seahorse Bioscience). Briefly, 4×10^4 cells were seeded in each well of a Seahorse XF 24 plate and incubated overnight. The following day, the cells were preincubated at 37 °C for a minimum of 45 min in the absence of CO_2 in RPMI (Seahorse, Agilent) with 25 mM glucose (Vicemed, Xuzhou, China) and 1 mM pyruvate (Vicemed) with the pH adjusted to 7.4.

Liquid chromatography-Mass spectrometry (LC-MS) and Proteomics analysis

The culture medium of *F. rodentium* or protein samples incubated with anti-flag M2 magnetic beads (M8823, Sigma) were harvested and separated on 4-12% gradient sodium dodecyl sulfate polyacrylamide gel electrophoresis (SDS-PAGE) gels. After being stained using Coomassie blue stain, the gel lanes were cut, harvested and subjected to peptide analysis [56]. The

proteomics analysis data were analyzed using the Majorbio Cloud Platform (www.majorbio.com).

Immunofluorescence staining and confocal microscopy

Cells or sections (5 μm) of paraffin-embedded tissues were stained with the indicated antibodies using a PANO 7-plex IHC kit (PANO) [54]. The analyses were performed using confocal laser scanning microscope (CLSM, Leica STELLARIS 5, Germany). The antibodies used are listed in Table S1.

Protein-Protein Docking

Protein PDB files were retrieved from UniProtKB. ACT and potential its receptor docking was performed using the GRAMM platform (version 2.6) with rigid-body docking parameters. This approach maintains fixed conformations for both ligand and receptor proteins while sampling complementary binding surfaces. Three-dimensional structures were generated through homology modeling via SWISS-MODEL, and the resulting PDB files were used as docking inputs. The simulation yielded 10 binding poses, with the top-ranked conformation selected based on ΔiG value.

Immunoblotting and Co-IP assay

Immunoblotting and Co-IP were performed as described [54]. The antibodies used are listed in Table S1.

Behavioral tests

The object location, novel object recognition, and elevated plus maze tests were executed to examine the effects of rACT protein on recognition memory

and anxiety-like behaviors of mice as described previously [57].

SLC25A22 expression

SLC25A22 expression in different cell types was assessed using the online database Tumor Immune Single-cell Hub 2 (TISCH2, https://tisch.compbio.cn).

Statistical analysis

Glutamine supplementation and lung metastasis model were performed once. rACT treatment experiments were repeated twice. The data were processed using SPSS25.0 statistical software, and the measurement data are expressed as mean ± standard deviation (mean ± SD). One-way ANOVA followed by LSD was used to test pairwise comparisons between groups, and t-tests for two-group comparisons. Statistical graphs were plotted using the GraphPad Prism software (version 9.0). $P < 0.05$ was considered statistically significant (*$P < 0.05$, **$P < 0.01$, ***$P < 0.001$).

Acknowledgments

We are grateful to Dr. Fuxing Dong (Xuzhou Medical University) for his technical support. We are also thankful to Professor Renjin Chen (Xuzhou Medical University) for providing NSG mice.

Author contributions

Conceptualization: Y.C., R.H.J., Y.C.P., J.Y.; Methodology: Y.C., R.H.J., H.Y.Z., B.B.J.,Y.C.P., J.Y.; Investigation: Y.C., R.H.J.,Y.H.X., C.Z., L.H.H., G.J.Z., H.G., B.B.J.,M.M.S.; Writing-original draft: Y.C., J.H.; Writing-review and editing: Y.C.P., J.Y.; Visualization: Y.C., R.H.J., J.H., Y.C.P.; Supervision: Y.C.P., J.Y.; Funding acquisition: R.H.J.,Y.C.P., J.Y.

Funding

This research was supported by the Natural Science Foundation of China (82471910 to J.Y.,82502134 to Y.C.P.), the Foundation for Universities of Jiangsu Province (No. 23KJA310011 to J.Y.), the Postgraduate Research & Practice Innovation Program of Jiangsu Province (26CXJH5207 to R.H.J.). This work was supported by the Jiangsu Distinguished Professorship Program to J.Y.

Data Availability

All data supporting the findings of this study are available within the paper and

its supplementary information files. Since the data of anti-tumor molecules in FCM, proteomics analysis and metabolic flux analysis, are still required for ongoing studies, they have not been deposited in a public database at this time. Additional data related to this paper are available from the corresponding author on reasonable request.

Declarations

Ethics approval and consent to participate

All animal experiments were performed under protocol (Approval No. 202104A077, 202303T015), which was reviewed and approved by the Research Ethics Committee of Xuzhou Medical University.

Consent to Participate: not applicable.

Competing interests

J.Y., H.Y.Z., and Y.C.P. filed a patent on the application of *F. rodentium* and its metabolites in HSC protection. J.Y., Y.C.P., Y.C., R.H.J. filed a patent on the application of *F. rodentium*-derived ACT protein in cancer suppression. The other authors declare that no competing interests exist.

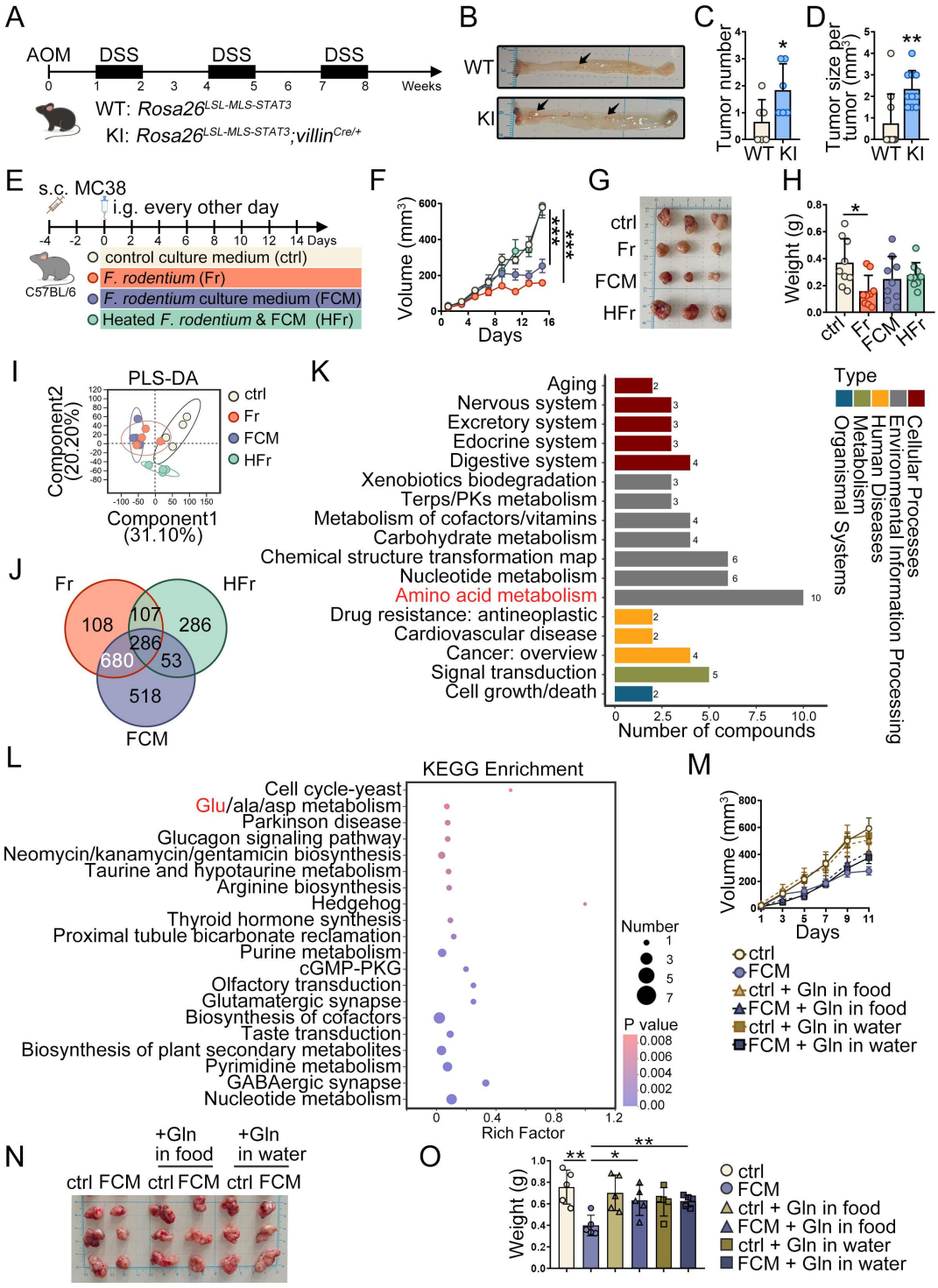

Figure 1. *F. rodentium*/FCM suppresses CRC development by reducing glutamate metabolism. (**A-D**) *Rosa26*$^{mSTAT3/mSTAT3}$ mice and *Rosa26*$^{mSTAT3/mSTAT3}$;*Villin*$^{Cre/+}$ mice were i.p. injected of 10 mg/kg AOM, and followed by three cycles of DSS treatment. At the end of experiment, the intestinal and colon sections

were removed, washed with PBS and opened longitudinally for analysis. (A) Experimental procedure for the establishment of the ulcerative colitis-related CRC model. (B) Representative morphological features of the tumors in colons from the AOM/DSS model. Tumor number (C) and tumor sizes (D) were recorded. The figures show the combination of twice experiments. (**E-H**) Tumor-bearing mice were treated with control culture medium, *F. rodentium*, FCM or HFr every other day (E). Tumor growth was monitored (F). At the end of the experiment, tumors were photographed (G) and tumor weights (H) were recorded. (**I**) The partial least squares-discriminant analysis (PLS-DA) of metabolite profiles by untargeted metabolomics analysis. (**J**) Venn diagram of the differentially abundant metabolites common to *F. rodentium* and FCM treatments. (**K-L**) KEGG pathway classification of the 680 differentially abundant metabolites. (**M-O**) Tumor-bearing mice were treated with control culture medium or FCM every other day, with dietary glutamine or glutamine in drinking water. Tumor growth was monitored (M). At the end of experiment, tumors were photographed (N) and tumor weights (O) were recorded. The figures shown represent a single experiment. *, P <0.05, **, P <0.01, ***,P <0.001.

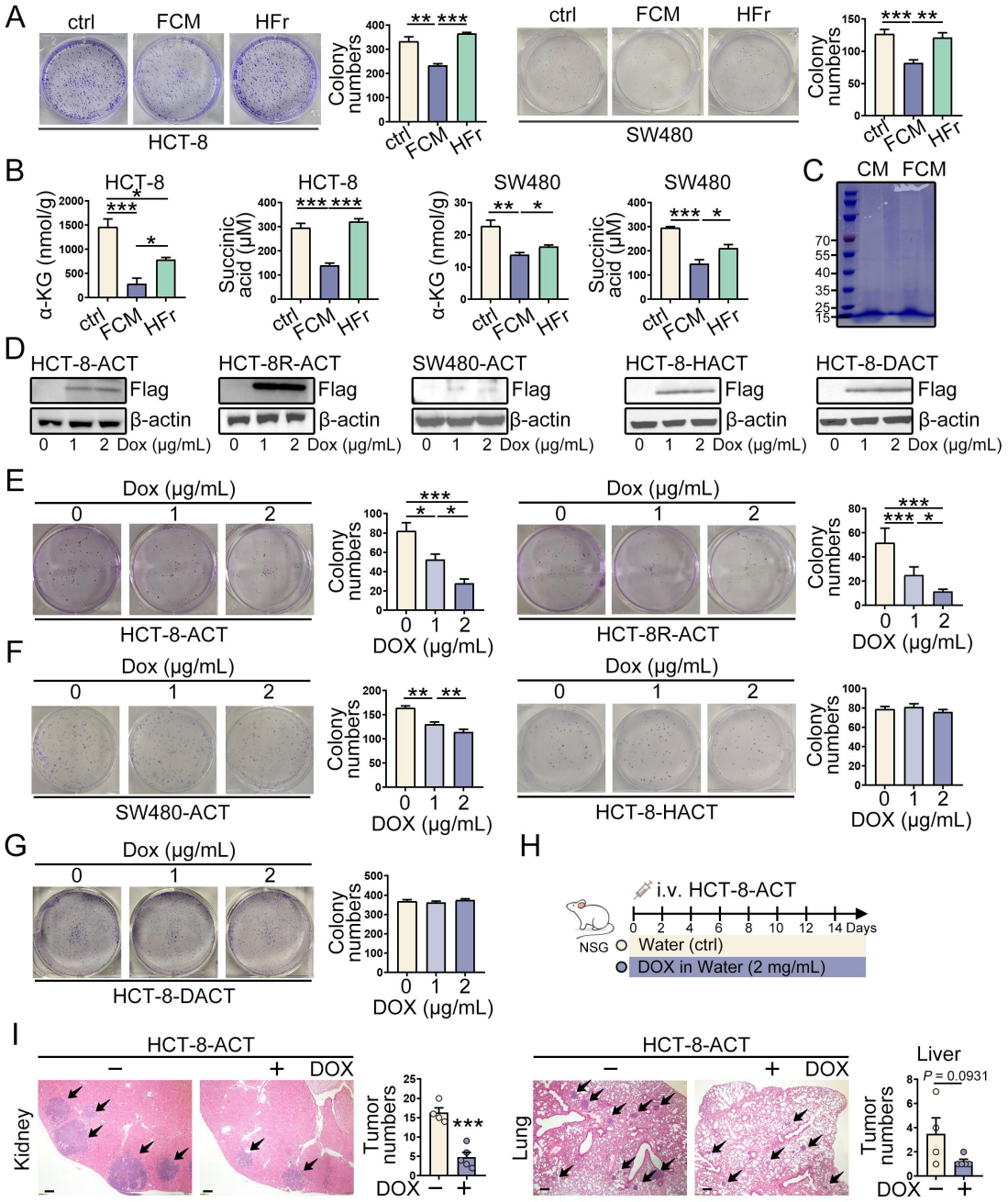

Figure 2. Ectopic expressing of ACT protein derived from *F. rodentium* inhibits CRC growth *in vitro* and *in vivo*. (**A**) HCT-8 and SW480 cells were pre-incubated with control culture medium, FCM or hFr, 6 h later, the cells were harvested and seed into the 6-well plates. After 7 - 10 days, the number of colonies was counted. (**B**) HCT-8 and SW480 cells were pre-incubated with control culture medium, FCM or hFr, 6 h later, the cells were harvested, and

the levels of α-KG and succinic acid in these cells were examined. (A-B) The data shown are representative of one of two independent experiments. (**C**) The proteins in control culture medium or FCM were separated by SDS-PAGE. CBB staining was performed and followed by LC-MS to investigate the potential receptor for ACT protein. The figure shown represent a single experiment. (**D**) CRC cell lines were infected with a lentivirus expressing ACT protein and treated with various concentration of DOX for 48 h. After which, the proteins were harvested, and subjected to Western blotting to examine the levels of Flag-ACT protein and β-actin. (**E-G**) CRC cell lines were infected with a lentivirus expressing ACT protein and treated with various concentration of DOX. After 7 - 10 days, the number of colonies was counted. (D-G) The data shown are representative of one of two independent experiments. (**H-I**) HCT-8 cells expressing ACT protein were transplanted into NSG mice and given normal water (n = 4) or water containing 2 mg/mL DOX (n = 5). After 21 days, the mice were euthanized, and major organs including lungs, liver and kidneys were removed, and embedded in paraffin for H&E staining. The figures shown represent a single experiment. *, P <0.05, **, P <0.01, ***,P <0.001.

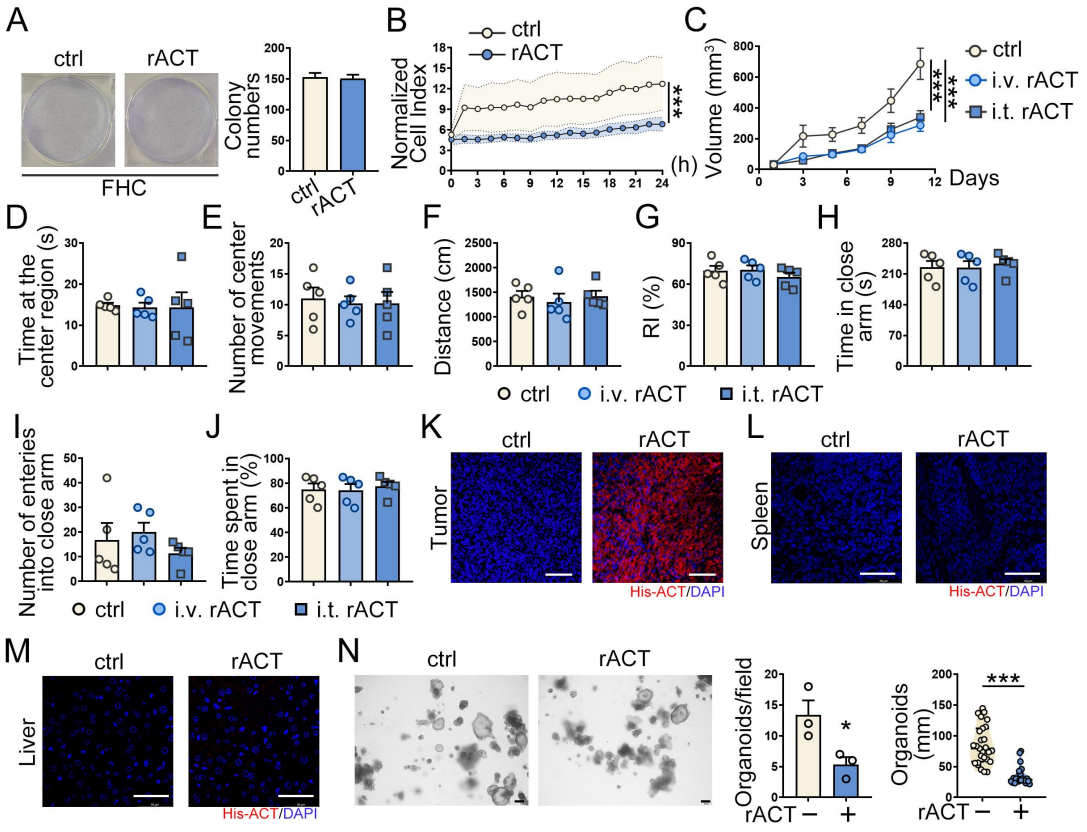

Figure 3. rACT protein inhibits CRC growth *in vitro* and *in vivo*. (**A**) FHC cells were treated with 1 μg/mL rACT. Every other day, the culture medium was replaced with fresh culture medium containing 1 μg/mL rACT. 7 - 10 days later, the number of colonies was counted. (**B**) SW480 cells (5000/well) were seeded and placed in an RTCA device at 37°C with 5% CO_2 to monitor and record the cell index. (**C**) Tumor-bearing mice were treated with either PBS or rACT (100 μg/tumor by intratumoral (i.t.) injection, or 5 mg/kg by i.v. injection). Tumor growth was monitored every other day. (A-C) The data shown are representative of one of two independent experiments. (**D-J**) After the last treatment, the cognitive function in tumor-bearing mice was examined. (**K-M**) At the end of the experiment, tumors and major organs from tumor-bearing mice treated with control or rACT by i.v. injection were removed and subjected

to IF to assess the His-tag ACT protein levels. (**N**) Organoids were seeded in culture medium and treated with or without rACT. 6 days later, the number and sizes of organoids were assessed. (D-L) The figures shown represent a single experiment. *, P <0.05, **, P <0.01, ***,P <0.001.

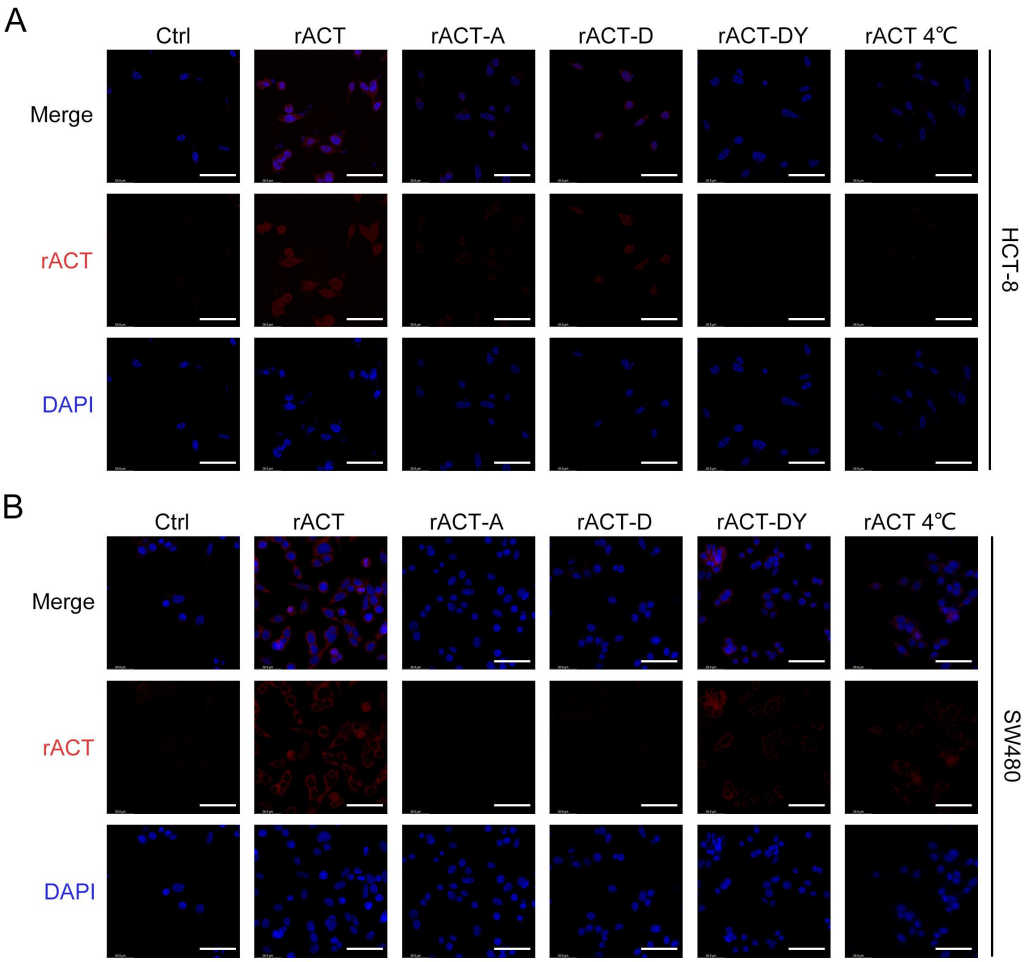

Figure 4. ACT enters cells via macropinocytosis. (**A-B**) HCT-8 cells (A) or SW480 cells (B) were treated with or without rACT (1 μg/mL, 0.5 h) in the presence or presence of Dynasore (80 μM, 0.5 h), Amiloride hydrochloride (30 μM, 0.5 h) and Cytochalasin D (5 μM, 1 h) to block clathrin-mediated endocytosis, macropinocytosis, and multiple endocytic and phagocytic

processes, respectively. The data shown are representative of one of two independent experiments. Bar, 10 μM. Red, His-tagged ACT protein; Blue, DAPI.

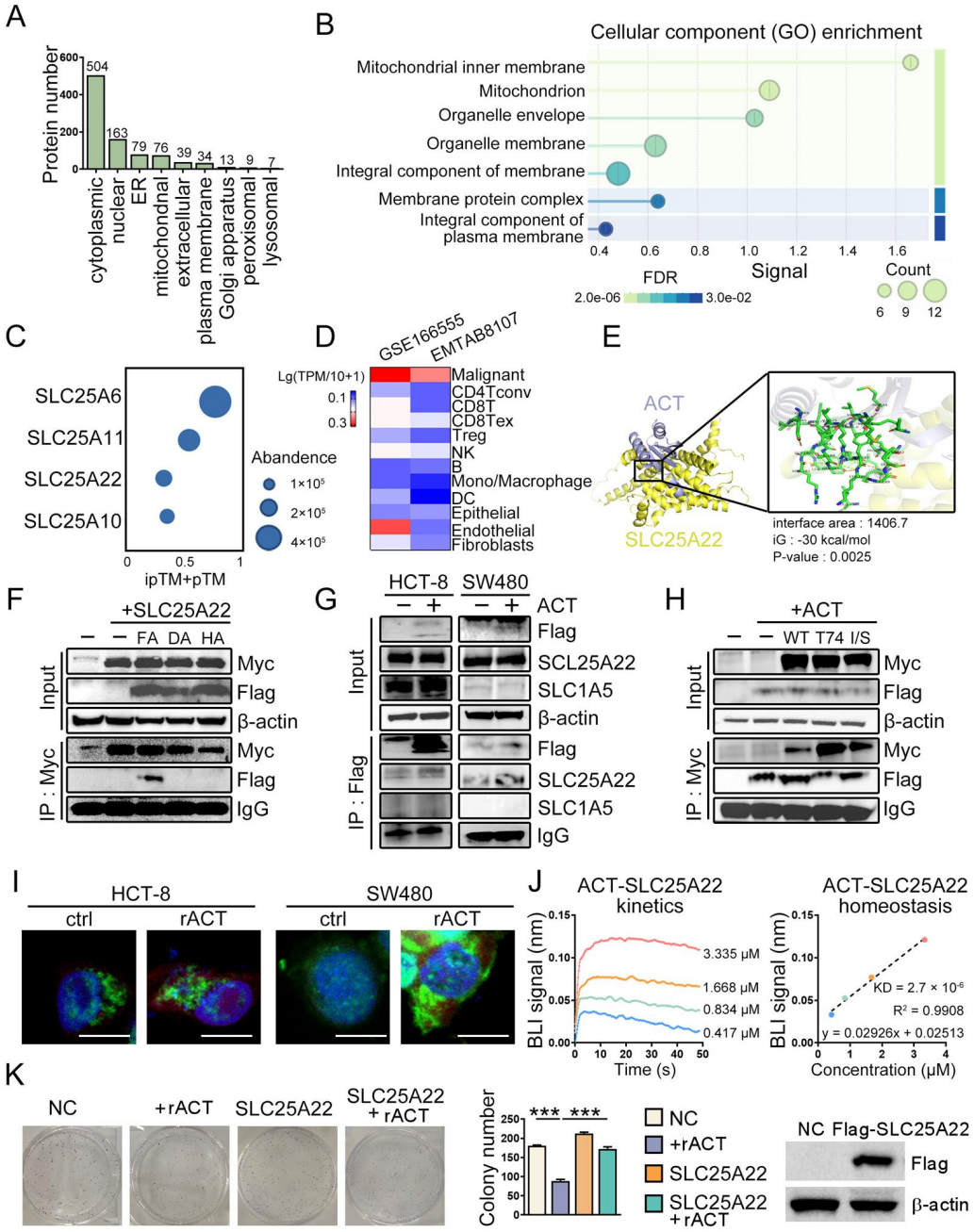

Figure 5. ACT directly interacts with SLC25A22. (**A**) HEK293T cells were transfected with either an empty vector or a plasmid coding Flag-ACT protein.

Proteins were harvested, incubated with an anti-Flag antibody, and subjected to LC/MS analysis to identify the potential receptor for ACT protein.(**B**) GO enrichment overview of mitochondrial protein. (**C**) The abundance of mitochondrial inner membrane protein. (**D**) The relative expression of SLC25A22 in various cell types was analyzed using using the online database TISCH2. (A-D) The data shown are representative of a single experiment. (**E**) The binding of ACT protein and SLC25A22 was predicted. (**F**) HEK293T cells transfected with a plasmid coding Flag-ACT protein were treated with or without 1 μg/mL DOX for 48 h, and followed by IP with an anti-Flag antibody to examine the interaction between Flag-ACT protein from different bacteria and SLC25A22. (**G**) HCT-8 cells or SW480 cells were transfected with a plasmid coding Flag-ACT protein, and followed by IP with an anti-Flag antibody to examine the interaction between Flag-tagged ACT protein and endogenous SLC25A22 or SLC1A5. (**H**) HEK293T cells were transfected with a plasmid coding Flag-ACT protein and/or the indicated mutant SLC25A22 plasmid, treated with 1 μg/mL DOX for 48 h, and followed by IP with an anti-Flag antibody to examine the interaction between Flag-tagged ACT protein and Myc-SLC25A22. (F-H) The data shown are from one of two independent experiments. (**I**) IF analysis to show the localization of ACT protein and SLC25A22. Bar, 10 μM. Red, His-tagged ACT protein; Green, SLC25A22; Blue, DAPI. (**J**) BLI experiments verified the interaction between ACT protein and SLC25A22. The rACT protein was immobilized on the biosensor, and the

sensor was immersed in the solutions containing different concentrations of purified SLC25A22 protein. The data shown are representative of a single experiment. (**K**) SW480 cells were transfected with Flag-SLC25A22 and selected with puromycin. Western blotting examined the Flag expression. The selected SW480 cells expressing Flag-SLC25A22 were treated with 1 μg/mL rACT. Every other day, the culture medium was replaced with fresh culture medium containing 1 μg/mL rACT. 7-10 days later, the number of colonies was counted. The data shown are representative of one of two independent experiments. *, P <0.05, **, P <0.01, ***,P <0.001.

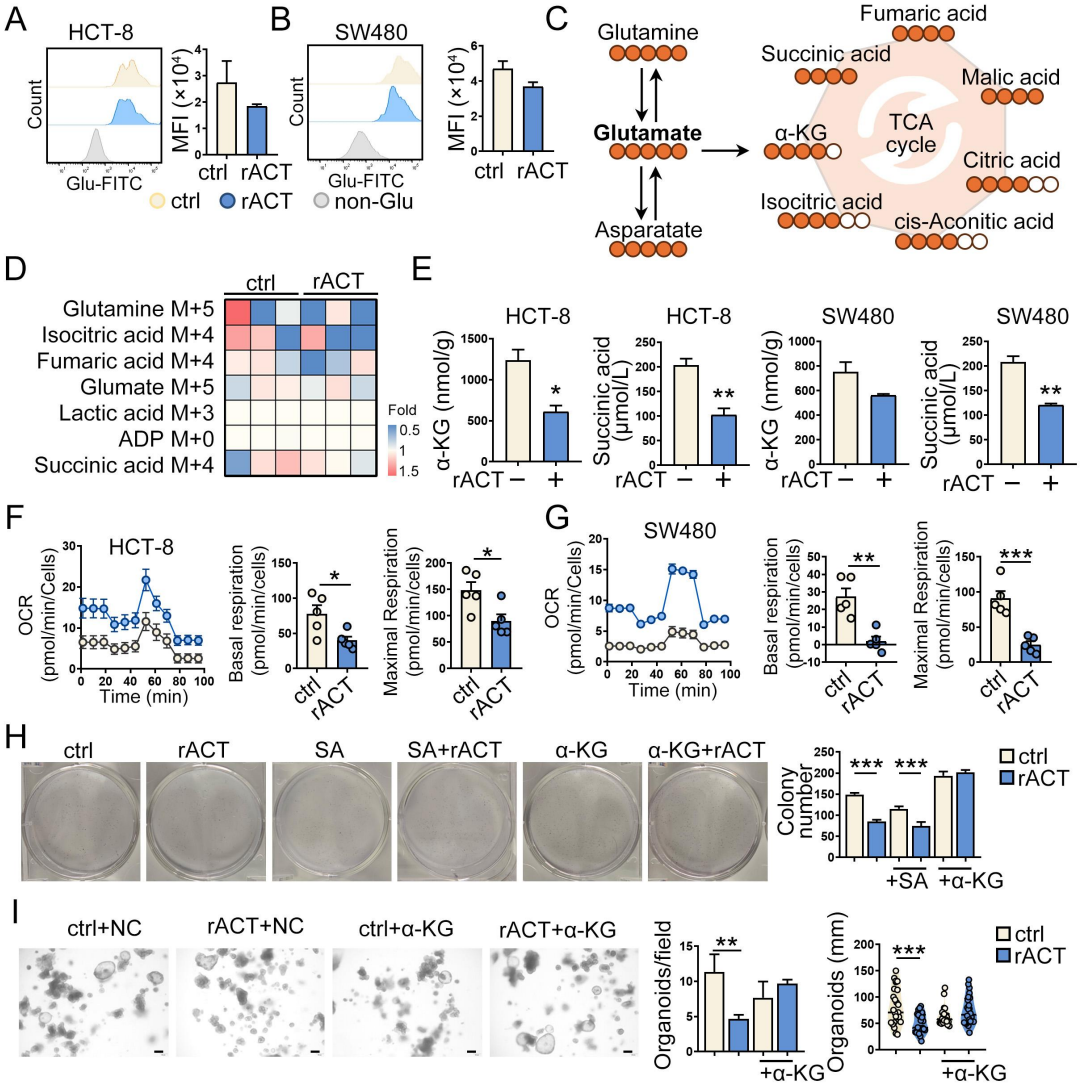

Figure 6. ACT reduces SLC25A22-mediated glutamate transport and metabolism. (**A-B**) CRC cell lines were treated with or without rACT (1 μg/mL) and subjected to flow cytometry to examine the FITC-glutamate uptake. The data shown are representative of one of two independent experiments. (**C**) Schematic diagram showing glutamate metabolic flux analysis in CRC cells. (**D**) ^{13}C-glutamate, ^{13}C-glutamine, ^{13}C-fumaric acid, ^{13}C-isocitric acid, ^{13}C-lactatic acid, and ^{13}C-ADP enrichment of HCT-8 cells treated with or without rACT for 24 hrs. The figures shown represent a single experiment. (**E**) The levels of α-KG and succinic acid in CRC cell lines were examined in the presence or

absence of rACT. The data shown are representative of one of two independent experiments. (**F-G**) The basal and maximal OCRs were analyzed by Seahorse. The figures shown represent a single experiment. (**H**) SW480 cells harboring KRAS mutations were treated with the indicated compounds, and the number of colonies was counted. The data shown are representative of one of two independent experiments. (**I**) Organoids were seeded in the culture medium and treated with or without rACT in the presence or absence of α-KG. 6 days later, the number and sizes of organoids were assessed. The figures shown represent a single experiment. *, P <0.05, **, P <0.01, ***,P <0.001.

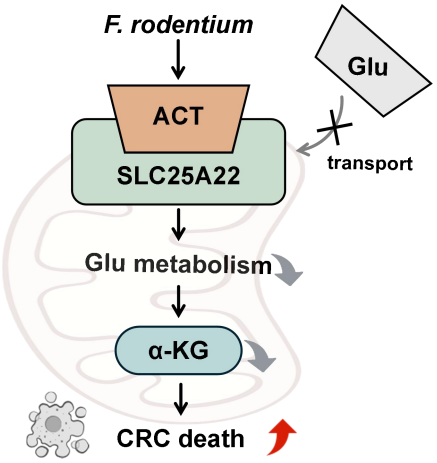

Figure 7. The model shows the anti-tumor effects and underlying mechanisms of ACT protein. ACT protein derived from *F. rodentium* is actively internalized into tumor cells by un-classical pathway, and then directly binds to SLC25A22 to reduce SLC25A22-mediated glutamate transport and metabolism, which subsequently in turn suppresses CRC development.

References

1. E. Morgan, M. Arnold, A. Gini, Lorenzoni, C. J. Cabasag, M. Laversanne, J. Vignat, J. Ferlay, N. Murphy and F. Bray, *Global burden of colorectal cancer in 2020 and 2040: incidence and mortality estimates from GLOBOCAN.* Gut, 2023. **72**(2): p. 338-344.
2. Y. H. Xie, Y. X. Chen and J. Y. Fang, *Comprehensive review of targeted therapy for colorectal cancer.* Signal Transduction and Targeted Therapy, 2020. **5**(1): p. 22.
3. C. C. Wong and J. Yu, *Gut microbiota in colorectal cancer development and therapy.* Nature Reviews Clinical Oncology, 2023. **20**(7): p. 429-452.
4. O. O. Coker, C. Liu, W. K. K. Wu, S. H. Wong, W. Jia, J. J. Y. Sung and J. Yu, *Altered gut metabolites and microbiota interactions are implicated in colorectal carcinogenesis and can be non-invasive diagnostic biomarkers.* Microbiome, 2022. **10**(1).
5. M. Y. Cao, Y. Deng, Q. Hao, H. Y. Yan, Q. L. Wang, C. Y. Dong, J. Wu, Y. J. He, L. B. Huang, X. Y. Xia, Y. C. Gao, H. N. Chen, W. H. Zhang, Y. J. Zhang, X. Z. Zhuo, L. Z. Dai, H. B. Hu, Y. Peng, F. Zhang, Z. Q. Liu, W. H. Huang, H. Y. Zhang, L. Yang, Y. Shu, W. Zhang, Y. Zhang and H. Xu, *Single-cell transcriptomic analysis reveals gut microbiota-immunotherapy synergy through modulating tumor microenvironment.* Signal Transduction and Targeted Therapy, 2025. **10**(1).
6. M. Zepeda-Rivera, S. S. Minot, H. Bouzek, H. R. Wu, A. Blanco-Míguez, P. Manghi, D. S. Jones, K. D. LaCourse, Y. Wu, E. F. McMahon, S. N. Park, Y. K. Lim, A. G. Kempchinsky, A. D. Willis, S. L. Cotton, S. C. Yost, E. Sicinska, J. K. Kook, F. E. Dewhirst, N. Segata, S. Bullman and C. D. Johnston, *A distinct clade dominates the colorectal cancer niche.* Nature, 2024. **628**(8007): p. 424-432.
7. T. C. Yu, F. F. Guo, Y. N. Yu, T. T. Sun, D. Ma, J. X. Han, Y. Qian, I. Kryczek, D. F. Sun, N. Nagarsheth, Y. X. Chen, H. Y. Chen, J. Hong, W. P. Zou and J. Y. Fang, *Fusobacterium nucleatum Promotes Chemoresistance to Colorectal Cancer by Modulating Autophagy.* Cell, 2017. **170**(3): p. 548-563.
8. G. Serna, F. Ruiz-Pace, J. Hernando, L. Alonso, R. Fasani, S. Landolfi, R. Comas, J. Jimenez, E. Elez, S. Bullman, J. Tabernero, J. Capdevila, R. Dienstmann and P. Nuciforo, *persistence and risk of recurrence after preoperative treatment in locally advanced rectal cancer.* Annals of Oncology, 2020. **31**(10): p. 1366-1375.
9. M. Jans and L. Vereecke, *Physiological drivers of pks plus E. coli in colorectal cancer.* Trends in Microbiology, 2025. **33**(9): p. 1003-1017.
10. H. Sokol, B. Pigneur, L. Watterlot, O. Lakhdari, L. G. Bermudez-Humarán, J. J. Gratadoux, S. Blugeon, C. Bridonneau, J. P. Furet, G. Corthier, C. Grangette, N. Vasquez, P. Pochart, G. Trugnan, G. Thomas, H. M. Blottière, J. Doré, P. Marteau, P. Seksik and P. Langella, *is an anti-inflammatory commensal bacterium identified by gut microbiota analysis of Crohn disease patients.* Proceedings of the National Academy of Sciences of the United States of America, 2008. **105**(43): p. 16731-16736.
11. M. Nshanian, J. J. Gruber, B. S. Geller, F. Chleilat, S. M. Lancaster, S. M. White, L. Alexandrova, J. M. Camarillo, N. L. Kelleher, Y. M. Zhao and M. P. Snyder, *Short-chain fatty acid metabolites propionate and butyrate are unique epigenetic regulatory elements linking diet, metabolism and gene expression.* Nature Metabolism, 2025. **7**(1): p. 196-211.

12. A. Montalban-Arques, E. Katkeviciute, P. Busenhart, A. Bircher, J. Wirbel, G. Zeller, Y. Morsy, L. Borsig, J. F. G. Garzon, A. Müller, I. C. Arnold, M. Artola-Boran, M. Krauthammer, A. Sintsova, N. Zamboni, G. E. Leventhal, L. Berchtold, T. de Wouters, G. Rogler, K. Baebler, M. Schwarzfischer, L. Hering, I. Olivares-Rivas, K. Atrott, C. Gottier, S. Lang, O. Boyman, R. Fritsch, M. G. Manz, M. R. Spalinger and M. Scharl, *Commensal strains mediate effective anti-cancer immune response against solid tumors.* Cell Host & Microbe, 2021. **29**(10): p. 1573-1588.
13. N. Sugimura, Q. Li, E. S. H. Chu, H. C. H. Lau, W. Fong, W. X. Liu, C. Liang, G. Nakatsu, A. C. Y. Su, O. O. Coker, W. K. K. Wu, F. K. L. Chan and J. Yu, *modulates the gut microbiota and produces anti-cancer metabolites to protect against colorectal tumourigenesis.* Gut, 2022. **71**(10): p. 2011-2021.
14. H. N. Bell, R. J. Rebernick, J. Goyert, R. Singhal, M. Kuljanin, S. A. Kerk, W. Huang, N. K. Das, A. Andren, S. Solanki, S. L. Miller, P. K. Todd, E. R. Fearon, C. A. Lyssiotis, S. P. Gygi, J. D. Mancias and Y. T. M. Shah, *Reuterin in the healthy gut microbiome suppresses colorectal cancer growth through altering redox balance.* Cancer Cell, 2022. **40**(2): p. 185-200.
15. L. J. Wang, L. Tang, Y. M. Feng, S. Y. Zhao, M. Han, C. Zhang, G. H. Yuan, J. Zhu, S. Y. Cao, Q. Wu, L. Li and Z. Zhang, *A purified membrane protein from or the pasteurised bacterium blunts colitis associated tumourigenesis by modulation of CD8⁺ T cells in mice.* Gut, 2020. **69**(11): p. 1988-1997.
16. Q. Li, W. Hu, W. X. Liu, L. Y. Zhao, D. Huang, X. D. Liu, H. Chan, Y. C. Zhang, J. D. Zeng, O. O. Coker, W. Kang, S. S. M. Ng, L. Zhang, S. H. Wong, T. Gin, M. T. V. Chan, J. L. Wu, J. Yu and W. K. K. Wu, *Streptococcus thermophilus Inhibits Colorectal Tumorigenesis Through Secreting β-Galactosidase.* Gastroenterology, 2021. **160**(4): p. 1179-1193.
17. S. Viaud, F. Saccheri, G. Mignot, T. Yamazaki, R. Daillère, D. Hannani, D. P. Enot, C. Pfirschke, C. Engblom, M. J. Pittet, A. Schlitzer, F. Ginhoux, L. Apetoh, E. Chachaty, P. L. Woerther, G. Eberl, M. Bérard, C. Ecobichon, D. Clermont, C. Bizet, V. Gaboriau-Routhiau, N. Cerf-Bensussan, P. Opolon, N. Yessaad, E. Vivier, B. Ryffel, C. O. Elson, J. Doré, G. Kroemer, P. Lepage, I. G. Boneca, F. Ghiringhelli and L. Zitvogel, *The Intestinal Microbiota Modulates the Anticancer Immune Effects of Cyclophosphamide.* Science, 2013. **342**(6161): p. 971-976.
18. T. Tanoue, S. Morita, D. R. Plichta, A. N. Skelly, W. Suda, Y. Sugiura, S. Narushima, H. Vlamakis, I. Motoo, K. Sugita, A. Shiota, K. Takeshita, K. Yasuma-Mitobe, D. Riethmacher, T. Kaisho, J. M. Norman, D. Mucida, M. Suematsu, T. Yaguchi, V. Bucci, T. Inoue, Y. Kawakami, B. Olle, B. Roberts, M. Hattori, R. J. Xavier, K. Atarashi and K. Honda, *A defined commensal consortium elicits CD8 T cells and anti-cancer immunity.* Nature, 2019. **565**(7741): p. 600-605.
19. H. Y. Zhu, H. Guo, N. Sun, R. Xiao, B. B. Ji, R. H. Jiang, F. X. Dong, C. Yao, X. R. Wang, R. Q. Li, J. Zhao, X. Q. Li, S. Z. Gong, Y. Q. Qin, X. Chen, Y. C. Pan, T. Ikezoe and J. Yang, *Faecalibaculum rodentium Alleviates Ionizing Radiation-Induced Damage in Mice by Improving Intestinal Integrity and Hematopoiesis via Its Metabolite Butyrate.* Advanced Science, 2026. **12**(2): p. e09383.
20. E. Zagato, C. Pozzi, A. Bertocchi, T. Schioppa, F. Saccheri, S. Guglietta, B. Fosso, L. Melocchi, G. Nizzoli, J. Troisi, M. Marzano, B. Oresta, I. Spadoni, K. Atarashi, S. Carloni, S. Arioli, G. Fornasa, F. Asnicar, N. Segata, S. Guglielmetti, K. Honda, G. Pesole, W. Vermi, G.

Penna and M. Rescigno, *Endogenous murine microbiota member and its human homologue protect from intestinal tumour growth.* Nature Microbiology, 2020. **5**(3): p. 511-524.

21. S. M. Jeong, S. Hwang, K. Park, S. Yang and R. H. Seong, *Enhanced mitochondrial glutamine anaplerosis suppresses pancreatic cancer growth through autophagy inhibition.* Scientific Reports, 2016. **6**: p. 30767.
22. L. Sainero-Alcolado, J. Liaño-Pons, M. V. Ruiz-Pérez and M. Arsenian-Henriksson, *Targeting mitochondrial metabolism for precision medicine in cancer.* Cell Death and Differentiation, 2022. **29**(7): p. 1304-1317.
23. N. A. P. Franken, H. M. Rodermond, J. Stap, J. Haveman and C. van Bree, *Clonogenic assay of cells.* Nature Protocols, 2006. **1**(5): p. 2315-2319.
24. D. L. Tang, J. Y. Wang, G. Kroemer and R. Kang, *Targeting macropinocytosis for cancer therapy.* Nature Reviews Cancer, 2026. **26**(3): p. 167-184.
25. K. Li and D. M. Underhill, *Phagocytosis: a process that shapes immune responses to engulfed meals.* Nature Reviews Immunology, 2026. **26**(4): p. 255-268.
26. Z. C. Le, Q. Pan, Z. P. He, H. Liu, Y. Shi, L. X. Liu, Z. J. Liu, Y. Ping and Y. M. Chen, *Direct Cytosolic Delivery of Proteins and CRISPR-Cas9 Genome Editing by Gemini Amphiphiles via Non-Endocytic Translocation Pathways.* Acs Central Science, 2023. **9**(7): p. 1313-1326.
27. B. Xie, S. P. Xu and S. Sivasankar, *Outside-in engineering of cadherin endocytosis using a conformation strengthening antibody.* Nature Communications, 2025. **16**(1): p. 1157.
28. J. S. Lee, H. Lee, S. Lee, J. H. Kang, S. H. Lee, S. G. Kim, E. S. Cho, N. H. Kim, J. I. Yook and S. Y. Kim, *Loss of SLC25A11 causes suppression of NSCLC and melanoma tumor formation.* Ebiomedicine, 2019. **40**: p. 184-197.
29. W. T. Li, L. Liang, S. Y. Liu, J. Q. Tang, S. Y. Ou, Z. J. Yuan, Y. H. Zhou and X. Yuan, *Inhibin beta A drives colorectal cancer progression through macrophage M2 polarization and mitochondria-dependent ferroptosis suppression.* Signal Transduction and Targeted Therapy, 2025. **10**(1): p. 420.
30. P. P. Ding, X. D. Huang, L. Shen, L. Du, X. C. Cheng, Y. X. Lu, H. Liu, D. D. Lin and F. J. Xiao, *PTPMT1 regulates mitochondrial death through the SLC25A6-NDUFS2 axis in pancreatic cancer cells.* American Journal of Cancer Research, 2023. **13**(3): p. 992-1003.
31. Q. M. Zhou, Y. Peng, F. F. Ji, H. R. Chen, W. Kang, L. S. Chan, H. Y. Gou, Y. F. Lin, P. M. Huang, D. Y. Chen, Q. Y. Wei, H. Su, C. Liang, X. Zhang, J. Yu and C. C. Wong, *Targeting of SLC25A22 boosts the immunotherapeutic response in KRAS-mutant colorectal cancer.* Nature Communications, 2023. **14**(1): p. 4677.
32. C. C. Wong, J. Y. Xu, X. Q. Bian, J. L. Wu, W. Kang, Y. Qian, W. L. Li, H. R. Chen, H. Y. Gou, D. B. Liu, S. T. Y. Luk, Q. M. Zhou, F. F. Ji, L. S. Chan, S. Shirasawa, J. J. Y. Sung and J. Yu, *In Colorectal Cancer Cells With Mutant KRAS, SLC25A22-Mediated Glutaminolysis Reduces DNA Demethylation to Increase WNT Signaling, Stemness, and Drug Resistance.* Gastroenterology, 2020. **159**(6): p. 2163-2180.
33. C. C. Wong, Y. Qian, X. N. Li, J. Y. Xu, W. Kang, J. H. Tong, K. F. To, Y. Jin, W. L. Li, H. R. Chen, M. Y. Y. Go, J. L. Wu, K. W. Cheng, S. S. M. Ng, J. J. Y. Sung, Z. W. Cai and J. Yu, *SLC25A22 Promotes Proliferation and Survival of Colorectal Cancer Cells With KRAS*

Mutations and Xenograft Tumor Progression in Mice via Intracellular Synthesis of Aspartate. Gastroenterology, 2016. **151**(5): p. 945-960.

34. H. X. Zhao, J. Park, Y. Z. Wang, Y. J. Chou, L. M. Li, L. N. Raines, M. Hsu, C. C. Lin, W. Cao, Y. L. Ouyang, H. Y. Chen, L. H. Zheng, Z. H. Li, A. Y. Huang, P. C. Ho, C. W. J. Lio and S. C. C. Huang, *Cancer suppresses mitochondrial chaperone activity in macrophages to drive immune evasion.* Nature Immunology, 2025. **26**(12): p. 2185-2200.
35. L. Lanzetti, *Oncometabolites at the crossroads of genetic, epigenetic and ecological alterations in cancer.* Cell Death and Differentiation, 2024. **31**(12): p. 1582-1594.
36. H. M. Zarour and G. Trinchieri, *Harnessing the Microbiome in Cancer Immunotherapy: Regulation, Prediction, and Therapeutic Targeting.* Annual Review of Immunology, 2026. **44**(1): p. 41-70.
37. P. Steppe, K. O'Connor and J. Hasty, *Rational engineering of combinatorial bacterial therapies for cancer.* Genome Biology, 2026. **27**(1): p. 53.
38. R. Kuru-Yasar and O. Üstün-Aytekin, *The Crucial Roles of Diet, Microbiota, and Postbiotics in Colorectal Cancer.* Current Nutrition Reports, 2024. **13**(2): p. 126-151.
39. B. A. Tegegne, D. Abebaw, Z. H. Teffera, A. Fenta, H. Belew, M. Belayneh, M. Jemal, M. Getinet, T. Baylie, F. B. Tamene, W. Y. Belay, S. A. Wondim and T. K. Zeleke, *Microbial Therapeutics in Cancer: Translating Probiotics, Prebiotics, Synbiotics, and Postbiotics From Mechanistic Insights to Clinical Applications: A Topical Review.* Faseb Journal, 2025. **39**(20): p. e71146.
40. S. K. Abdeen, I. Mastandrea, N. Stinchcombe, J. Puschhof and E. Elinav, *Diet-microbiome interactions in cancer.* Cancer Cell, 2025. **43**(4): p. 680-707.
41. J. Suez, N. Zmora, E. Segal and E. Elinav, *The pros, cons, and many unknowns of probiotics.* Nature Medicine, 2019. **25**(5): p. 716-729.
42. N. Zmora, G. Zilberman-Schapira, J. Suez, U. Mor, M. Dori-Bachash, S. Bashiardes, E. Kotler, M. Zur, D. Regev-Lehavi, R. B. Brik, S. Federici, Y. Cohen, R. Linevsky, D. Rothschild, A. E. Moor, S. Ben-Moshe, A. Harmelin, S. Itzkovitz, N. Maharshak, O. Shibolet, H. Shapiro, M. Pevsner-Fischer, I. Sharon, Z. Halpern, E. Segal and E. Elinav, *Personalized Gut Mucosal Colonization Resistance to Empiric Probiotics Is Associated with Unique Host and Microbiome Features.* Cell, 2018. **174**(6): p. 1388-1405.
43. L. Kern, A. Tofield, J. Frame and E. Elinav, *Next-generation probiotics: an outlook into current applications and future developments.* Nature Reviews Microbiology, 2026. **24**(8): p. 539-558.
44. X. J. Yang, M. Liu, T. Wang, X. J. Ma, Z. R. Guan, B. Ma, X. G. Duan and C. X. Su, *Gut-derived exerts anti-cancer effects on colorectal cancer by modulating PDPN-CLEC-2 signaling pathway.* Msystems, 2025. **10**(8): p. e0014825.
45. J. S. Liberles, M. Thórólfson and A. Martínez, *Allosteric mechanisms in ACT domain containing enzymes involved in amino acid metabolism.* Amino Acids, 2005. **28**(1): p. 1-12.
46. J. H. Kim, Y. J. Kang, Y. W. Kang, S. E. Park, H. B. Jin, E. Hong and H. H. Park, *A putative membrane-associated YdjB-like protein from exhibits a non-canonical ACT-like fold.* Plos One, 2025. **20**(12): p. e0336436.

47. G. Curien, V. Biou, C. Mas-Droux, M. Robert-Genthon, J. L. Ferrer and R. Dumas, *Amino acid biosynthesis: New architectures in allosteric enzymes.* Plant Physiology and Biochemistry, 2008. **46**(3): p. 325-339.
48. Y. Liu, Y. Wang, Z. Lin, R. Kang, D. L. Tang and J. Liu, *SLC25A22 as a Key Mitochondrial Transporter Against Ferroptosis by Producing Glutathione and Monounsaturated Fatty Acids.* Antioxidants & Redox Signaling, 2023. **39**(1-3): p. 166-185.
49. E. Goubert, Y. Mircheva, F. M. Lasorsa, C. Melon, E. Profilo, J. Sutera, H. Becq, F. Palmieri, L. Palmieri, L. Aniksztejn and F. Molinari, *Inhibition of the Mitochondrial Glutamate Carrier SLC25A22 in Astrocytes Leads to Intracellular Glutamate Accumulation.* Frontiers in Cellular Neuroscience, 2017. **11**: p. 149.
50. J. Han, Z. Jiang, C. N. Wang, X. Chen, R. Q. Li, N. Sun, X. Y. Liu, H. Wang, L. Hong, K. Y. Zheng, J. Yang and T. Ikezoe, *Inhibition of Aurora-A Promotes CD8 T-Cell Infiltration by Mediating IL10 Production in Cancer Cells.* Molecular Cancer Research, 2020. **18**(10): p. 1589-1602.
51. M. B. I. Gabra, Y. Yang, H. Li, P. Senapati, E. A. Hanse, X. H. Lowman, T. Q. Tran, L. S. Zhang, L. T. Doan, X. D. Xu, D. E. Schones, D. A. Fruman and M. Kong, *Dietary glutamine supplementation suppresses epigenetically-activated oncogenic pathways to inhibit melanoma tumour growth.* Nature Communications, 2020. **11**(1): p. 3326.
52. J. Han, X. Chen, J. W. Xu, L. L. Chu, R. Q. Li, N. Sun, Z. Jiang, H. Y. Liu, X. Ge, J. N. Zheng, J. Yang and T. Ikezoe, *Simultaneous silencing Aurora-A and UHRF1 inhibits colorectal cancer cell growth through regulating expression of DNMT1 and STAT1.* International Journal of Medical Sciences, 2021. **18**(15): p. 3437-3451.
53. R. Q. Li, N. Sun, X. Chen, X. Q. Li, J. Zhao, W. P. Cheng, H. Hua, M. Fukatsu, H. Mori, H. Takahashi, H. Ohkawara, M. Fukami, M. Okamoto, Y. Hamazaki, K. Y. Zheng, J. Yang and T. Ikezoe, *Mutation Promoted IL-6 Production and Glycolysis Mediating PKM1 Stabilization in Macrophages.* Frontiers in Immunology, 2021. **11**: p. 589048.
54. J. Zhao, C. Yao, Y. Q. Qin, H. Y. Zhu, H. Guo, B. B. Ji, X. Q. Li, N. Sun, R. Q. Li, Y. Z. Wu, K. Y. Zheng, Y. C. Pan, T. T. Zhao and J. Yang, *Blockade of C5aR1 resets M1 via gut microbiota-mediated PFKM stabilization in a TLR5-dependent manner.* Cell Death & Disease, 2024. **15**(2): p. 120.
55. X. Chen, N. Sun, R. Q. Li, X. J. Sang, X. Q. Li, J. Zhao, J. Han, J. Yang and T. Ikezoe, *Targeting HLA-F suppresses the proliferation of glioma cells via a reduction in hexokinase 2-dependent glycolysis.* International Journal of Biological Sciences, 2021. **17**(5): p. 1263-1276.
56. R. Q. Li, X. Q. Li, J. Zhao, F. D. Meng, C. Yao, E. S. Bao, N. Sun, X. Chen, W. P. Cheng, H. Hua, X. Y. Li, B. Wang, H. Wang, X. C. Pan, H. J. You, J. Yang and T. Ikezoe, *Mitochondrial STAT3 exacerbates LPS-induced sepsis by driving CPT1a-mediated fatty acid oxidation.* Theranostics, 2022. **12**(2): p. 976-998.
57. W. Pan, J. Zhao, J. Wu, D. Xu, X. Meng, P. Jiang, H. Shi, X. Ge, X. Yang, M. Hu, P. Zhang, R. Tang, N. Nagaratnam, K. Zheng, X. F. Huang and Y. H. Yu, *Dimethyl itaconate ameliorates cognitive impairment induced by a high-fat diet via the gut-brain axis in mice.* Microbiome, 2023. **11**(1): p. 30.